

Training nonlinear elastic functions: nonmonotonic, sequence dependent and bifurcating

Daniel Hexner

Faculty of Mechanical Engineering, Technion, 32000 Haifa, Israel

The elastic behavior of materials operating in the linear regime is constrained, by definition, to operations that are linear in the imposed deformation. Though the nonlinear regime holds promise for new functionality, the design in this regime is challenging. In this paper we demonstrate that a recent approach based on training [Hexner *et al.*, *PNAS* 2020, 201922847] allows responses that are inherently non-linear. By applying designer strains, a disordered solids evolves through plastic deformations that alter its response. We show examples of elaborate nonlinear training paths that lead to the following functions: (1) Frequency conversion (2) Logic gate and (3) Expansion or contraction along one axis, depending on the sequence of imposed transverse compressions. We study the convergence rate and find that it depends on the trained function.

I. INTRODUCTION

Recently, it has been realized that nontrivial functions can be imparted in ordinary disordered materials through small microscopic alterations[9, 11, 20, 27, 31]. This is believed to stem from the enormous design space defined by the accessible microstates. Originally conceived in tuning global material properties[9] (e.g., Poisson's ratio), it was then followed by designing spatially varying responses [21, 27, 28, 31] motivated by allostery in proteins. Both global and spatial dependent responses have been realized in simulations and experiment[26, 27].

Designing the microstructure often employs an optimization process to compute the structure. Realizing these designs, however, is challenging. It requires a precise knowledge of the interactions[26]. Scaling up the number of degrees becomes numerically expensive, while shrinking down the size of the microscopic elements necessitates control on tiny length scales.

To address these issues, an alternative has recently been proposed[24], termed "directed aging", which is based on the self-organization of microstructure. It considers disordered materials that deform plastically in response to applied strains. By applying carefully selected sequences of strains, material properties can be steered towards a desired goal. To date, this approach has been useful in manipulating global material properties in both simulations and experiment [13, 16, 24] (primarily the Poisson's ratio), as well as spatially varying allosteric responses in simulations[12].

In this paper we focus on the nonlinear regime, which allows behaviors that are inherently different than those in linear response [1, 2, 4, 5, 10, 15, 22]. We study the feasibility of training distinctly nonlinear responses by defining training sequences that couple source degrees of freedom to target degrees of freedom. Our aim is to realize a given strain on the target degrees of freedom in response to a strain on the source degrees of freedom. The training sequence defines curves (or training paths) in terms of the source and target strains. By devising elaborate training paths that are nonlinear, and may bifurcate, we are able to realize highly non-trivial responses:

1. frequency conversion 2. logic gates and 3. a material that either expands or contracts along one axis, depending on the sequences of applied compression. We study the convergence as a function of the number of training cycles and find that it is often very slow.

II. MODEL AND TRAINING PROCEDURE

We model an amorphous solid using a disordered network of springs whose the energy depends on the stiffness, k_i , the bond length ℓ_i and the rest length $\ell_{i,0}$:

$$U = \frac{k_i}{2} \sum_i (\ell_i - \ell_{i,0})^2. \quad (1)$$

We employ networks derived from packings, since their coordination number is easily tuned by the pressure exerted on the box[23]. Details of the network and packing preparation are defined in Appendix A. We allow plastic deformations that alter the structure through changes to the rest lengths[13]. The rest lengths of a bond is assumed to evolve in proportion to the stress it experiences:

$$\partial_t \ell_i = \gamma k_i (\ell_i - \ell_{i,0}). \quad (2)$$

A bond elongates under tension and shortens under compression. This model is essentially the Maxwell model for viscoelasticity[19]: each bond is a spring and dashpot in series, where the latter accounts for the change in rest length. We assume that the time to reach force balance can be neglected with respect to the viscous time scales.

For each response a target deformation and source deformation are defined, each with a corresponding strain ϵ_T and ϵ_S . These degrees of freedom may either be global (e.g., uniaxial strain) or local (e.g., squeezing a pair of nodes). Motion in the quasistatic regime follows low energy directions and therefore training aims at programming low energy "valleys" that steer the response. We follow the training procedure of Ref. [12] where the system is strained periodically along the prescribed training paths. We note that, Eq. 2 is the gradient of the energy

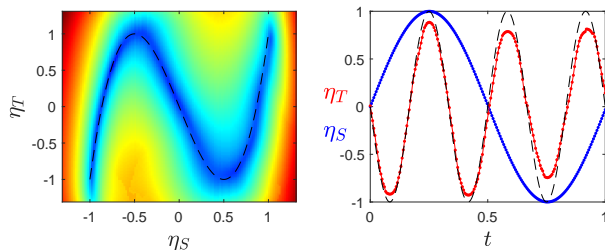


Figure 1. Frequency conversion through non-monotonic training path for allostery. Left: The elastic energy measured as a function of the source and target strains (normalized to the strain amplitude ϵ_{Age}). The energy landscape forms a valley along the trained path, $\eta_T = -3\eta_S + 4\eta_S^3$, marked by the dashed line. Right: The quasistatic response to an applied time periodic source strain. The parameters are the same as in Fig. 2.

with respect to the rest lengths, and therefore at a constant imposed strain minimizes the elastic energy at that strain. Straining periodically along a path $\epsilon_T = f(\epsilon_S)$ reduces the energy along that entire path, creating an energy valley. Actuating the source forces the system along that same curve $\epsilon_T = f(\epsilon_S)$.

We consider four examples of responses. Of these two are global responses, and two are spatially dependent that couple far away degrees of freedom.

III. RESULTS

A. Frequency conversion through non-monotonic paths

We begin by training a family of responses whose non-linearity can be tuned, interpolating between a linear function ($\alpha = 0$) and non-monotonic function ($\alpha > 1$):

$$\eta_T = (1 - \alpha)\eta_S + \alpha\eta_S^3. \quad (3)$$

For simplicity we have defined $\eta_S = \epsilon_S/\epsilon_{Age}$ and $\eta_T = \epsilon_T/\epsilon_{Age}$ where ϵ_{Age} is the strain amplitude, chosen to be the same on the source and target.

To demonstrate the generality of training nonlinear responses, we consider both the allostery inspired response [12, 27, 31] (Fig. 2 left) as well as global deformations (Fig. 2 right). The global degrees of freedom are the uniaxial strain; ϵ_S is the strain along the x-axis while ϵ_T is the strain along the y-axis. For the allosteric response the source and target degrees of freedom are pairs of nearby nodes, as illustrated in Fig 2 (a). Squeezing a pair of source nodes leads to a prescribed strain on the far away target nodes. The strain is defined as the fractional change in distance between a pair of nodes, $\epsilon = \frac{\ell - \ell_0}{\ell_0}$. To communicate strain over long distances we are limited to using near isostatic networks whose anomalous elasticity is long ranged [7, 12, 17].

We focus on $\alpha \leq 4$, where η_T is in the range $[-1, 1]$. The case of $\alpha = 4$ is particularly interesting, since applying a time dependent sinusoidal source strain $\eta_S = \sin(\omega t)$ yields $\eta_T = -\sin(3\omega t)$. As noted, during training both the source and targets are strained periodically which results in an energy valley that follows the training path. Fig.1(a) shows this energy landscape, as function of the source and target strains, for the case $\alpha = 4$ and allosteric degrees of freedom. To assess the success of training we then actuate the source degrees of freedom and measure the strain on the target. Fig.1(b) shows indeed that applying to the source a sinusoidal time dependent strain results in a response on the target at nearly triple the frequency. Other integer conversion ratios can be achieved by the appropriate polynomials. Thus, we are able to convert the frequency of the applied driving. We note however, the change in frequency is due to the non-monotonic energy valley – all our responses are in the quasistatic regime.

We now turn to discuss the behavior as a function of α . The success of training is characterized in Fig. 2(b) and (f) following the training period. We plot η_T as a function of the η_S averaged over approximately 50 of samples. On average the response is close to the training paths, denoted by the dashed lines. Training is more successful for small values of α .

To quantify the convergence of the response as a function of the number of training cycles we define a quantity $\delta\eta$ that measures the distance of the response from the intended value. We strain the source degrees of freedom, by varying the strain in M small strain steps, denoted with i and measure the deviation of η_T from the trained path:

$$(\delta\eta)^2 = \frac{1}{M} \sum_{i=1}^M \left(\eta_T^{(i)} - \eta_{T,path}^{(i)} \right)^2. \quad (4)$$

Fig. 2 (c) and (g) shows that the convergence time of $\delta\eta$ grows with α . Non-monotonic responses are more difficult to train, since they have a larger convergence time. At large times $\delta\eta$ decays approximately as a power-law, roughly scaling as $\tau^{\approx -0.5}$ for the allostery inspired response, and a quicker $\tau^{\approx -1.0}$ decay for the uniaxial strain.

Since training reduces the energy along the training paths, we also measure the elastic energy along the path as a function of the number of training cycles. Surprisingly, the α dependent time scale is not reflected in the relaxation of the energy. Fig. 2 (d) and (h) shows that the energy approximately scales as τ^{-1} independent of α . This appears to be a robust feature common to many of the examples considered. Below we present an argument for that scaling.

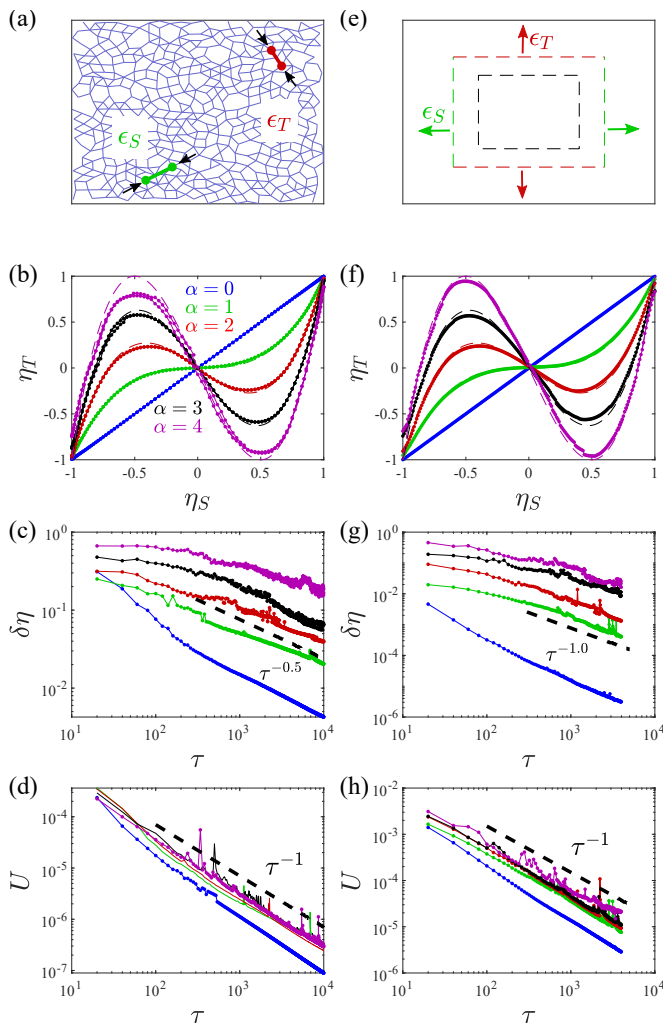


Figure 2. Training non-monotonic responses in allostery (left) and uniaxial response (right). (a) An illustration of the networks and the trained allostery inspired response. Squeezing the source sites leads to a prescribed motion in the target nodes. (e) The source and target strain in the global responses are defined to be the uniaxial global strain. (b), (f) The training paths are denoted by the dashed lines and the trained responses with the measured responses overlaid. (c) (g) The convergence of the trained response as a function of the number of training cycles. The asymptotic decay appears to be different for the global and local response (dashed line are a guide to the eye). (d),(h) shows the decays of the energy as function of the training cycles. For the global response we choose: $\epsilon_{Age} = 0.05$ and the aging rate $\Gamma = 16.0$. For the allosteric response $\epsilon_{Age} = 0.2$ and $\Gamma = 4.0$.

B. XOR gate via bifurcations

Within linear response applying two different strains results in a response that is the sum of the two individual responses. In the nonlinear regime this restriction does not apply. We consider logic gates with two inputs and a single output as an example as a non-additive mapping.

Here we aim at realizing the XOR gate (AND and OR can be realized using similar ideas). Logic gates were previously achieved by design of 3d-printed structures[14, 32].

The XOR gate is defined in Fig. 3(a) has two discrete inputs and a single output. Note that negating the two inputs does not negate the output. We assign two sources and a single target, each to a randomly chosen pair of adjacent nodes (as in allostery). The corresponding strain are η_{S1}, η_{S2} for the sources and η_T for the target. The four discrete state correspond to the maximal strain amplitude, where $|\eta_{S1}| = |\eta_{S2}| = 1$. Our goal is to train the system so that actuating the two source sites to one of the four states will yield $\eta_T = \pm 1$ as defined by the XOR gate. To train these responses we interpolate the discrete states into continuous paths that bifurcate from the unstrained state at the origin. The training paths, shown in Fig. 3(b), are composed of two curves: I) $\eta_T = -\eta_{S1}^2 = -\eta_{S2}^2$ with $\eta_{S1} = \eta_{S2}$, and II) $\eta_T = \eta_{S1}^2 = \eta_{S2}^2$ with $\eta_{S1} = -\eta_{S2}$. Note these curves only meet at the unstrained state ($\eta_{S1} = \eta_{S2} = \eta_T = 0$) and depending on the applied strains the system follows one of the four branches. We note that multi-branched responses have also been studied in Ref. [18, 25].

Fig. 3(b) shows the measured response after a large number of training cycles. As can be seen, it reasonably matches the training paths, denoted by the dashed curves. Fig. 3(c) shows $\delta\eta$ as a function of cycles; also here it decays as approximately as $\tau^{-0.5}$. The energy vs. number of cycles is shown in 3(d) approximately follows the τ^{-1} scaling. In this example we also test the effect of varying the aging rate, $\Gamma = \gamma k$, but find little change to the functional behavior.

C. Sequence dependent responses

We have shown that bifurcations allow the system to traverse different branches as a function of the two (or more) imposed strains. Here we consider a bifurcation where the branch is selected based on the order of applied strains, rather than their value. We consider a three dimensional system with two sources, defined to be the uniaxial deformation along the x and y direction, while target deformation is along the z-axis. The corresponding normalized strain along these directions are denoted by η_x, η_y and η_z . The goal of training is shown in Fig. 3(e): compressing along the x-axis and then the y-axis results in an expansion along the z-axis. Reversing the order of applied strains yields compression along the z-axis.

Such a response is realized through two training paths that bifurcate from the unstrained state, as shown in Fig. 3(f). Each sequence is composed of two linear segments: Seq A: $(\eta_x, \eta_y, \eta_z) \rightarrow (0, 0, 0) \rightarrow (1, 0, 0) \rightarrow (1, 1, 1)$. Seq B: $(\eta_x, \eta_y, \eta_z) \rightarrow (0, 0, 0) \rightarrow (0, 1, 0) \rightarrow (1, 1, -1)$. Because of the third dimension the two paths do not cross. To train such a path we alternate between training each of the two branches.

The measured response, η_z as a function of η_x and η_y is shown in Fig. 3(g) along with the training path (dashed curve). Training is successful, despite the sharp corner of the training path. Fig. 3(h) shows the convergence of the target response, $\delta\eta$ as a function of the number of the training cycles. Here, we consider the effect of varying the strain amplitude, ϵ_{Age} in the range of 2% to 6%. At the largest strain amplitude ϵ_{Age} training is highly successful and there is a clear sequence dependence. At small strains training is unsuccessful, suggesting that large strains are needed to access the non-linear regime.

We also plot the energy as a function of the number of cycles for the different strain amplitudes, ϵ_{Age} . Here, the functional dependence depends on ϵ_{Age} : while for small ϵ_{Age} it approximately scales as $\tau^{-1.0}$, at large strains it decays more slowly. Attaining this response at large strains is therefore more difficult, and since it is the only example that deviates from that convergence it could be an indicator of a new regime.

D. Evolution of the elastic energy

Over a broad range of parameters and training paths the energy along the training path decays approximately as τ^{-1} . We explain this trend through a simple argument. The change in rest length over a cycle scales as the force, or the energy divided by the strain: $\Delta\ell_0 \sim f\Delta\tau \propto U/\epsilon_{Age}\Delta\tau$. Assuming small deformations, the change in energy over a cycle is given by:

$$\Delta U = \frac{\partial U}{\partial \ell_0} \Delta \ell_0 \quad (5)$$

$$\sim -\frac{1}{a\epsilon_{Age}} U^2 \Delta\tau, \quad (6)$$

where we estimated the derivative by, $\frac{\partial U}{\partial \ell_0} \sim \frac{U}{a}$, and a is a microscopic length scale. Solving the differential equation yields $U \propto \epsilon_{Age}\tau^{-1}$ as observed. This also predicts the prefactor ϵ_{Age} , which is consistent with simulations.

IV. CONCLUSIONS

We have demonstrated that compound spring-dashpot bonded networks can be trained along highly nonlinear elaborate paths that curve and bifurcate. Our results are both valid for global responses as well as bond specific responses. These allow functionality that is usually not easily achieved by design. The nonmonotonic paths could possibly be used to transform the frequency of a signal. The bifurcating paths can be programmed to function as logic gates and allows materials whose response depends on the sequence of the imposed strains.

Though training is successful, the slowness of the dynamics hints at a difficulty. The convergence rate for the nonmonotonic responses becomes increasing slow as the

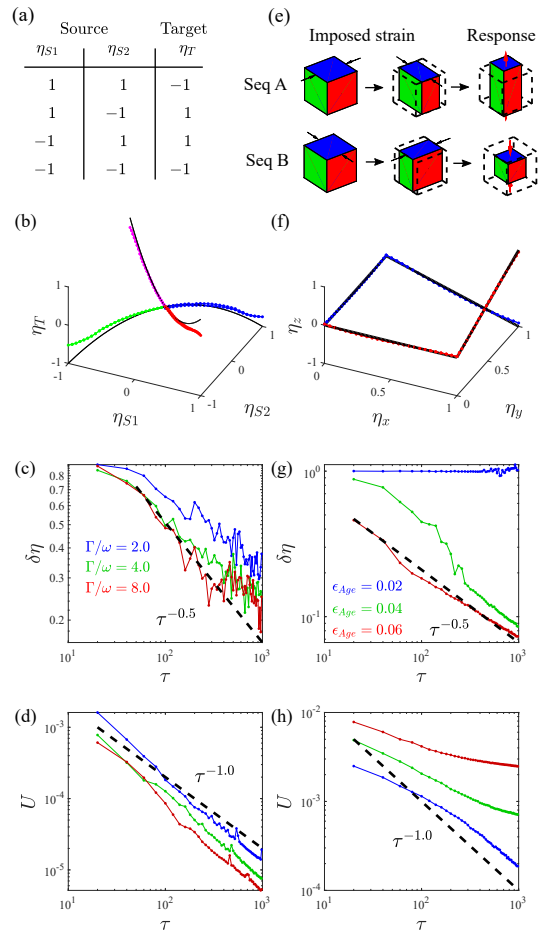


Figure 3. Left: Training the XOR logic gate define in (a) as an example of a non-additive response. Right: An example of a sequence dependent material, where the order of compressions along the x and y axis determine the response along the z axis (e). (b) and (f) the corresponding training paths. (c) and (g) the convergence of the response as a function of the number of training cycles. (d) and (h) the energy along the training path as a function of the number of training cycles. For the XOR gate we show that varying the aging rate $\Gamma = \gamma k$ with respect to training frequency ω has little effect. For the sequence dependent material small strains are less successful. Simulation parameters for XOR gate: $\epsilon_{Age} = 0.2$, average is over 20 realizations. For sequence dependent material $\Gamma = 2.0$ and 50 realizations.

path increasingly curves. The slow convergence could possibly be due to the unintentional formation of additional competing low energy modes[6, 29, 30]. The desired response is then only achieved when the energy along the target path is made smaller than the remaining competing directions. The density of states provides a rudimentary measurement of these low energy modes. In the Appendix B we show that indeed increasing α yields more low energy modes. Characterizing the entire energy landscape, however, is a difficult task. A different source of difficulty is seen in the slower than usual decay of the energy in the sequence dependent responses. This could

point to a new regime, where the system cannot attain the prescribed low energy mode, possibly an indication of a limit to the system's capacity.

ACKNOWLEDGEMENTS

We would like to thank Dov Levine, Andrea J. Liu, Sidney R. Nagel, Nidhi Pashine and Menachem Stern for enlightening discussions. We acknowledge the University of Chicago Research Computing Center for support of the initial steps of this work. We are grateful to the ATLAS cluster at the Technion for providing computing resources. This work was supported by the Israel Science Foundation (grant 2385/20).

APPENDIX A: NUMERICAL METHODS

Packing preparation

We prepare our networks from packings of soft spheres with repulsive harmonic interactions[8, 23]. For every pair of overlapping particles (the distance $|r_i - r_j|$ falls below the sum of the radii $R_i + R_j$) the energy is given by:

$$U_{ij} = \frac{k}{2} \sum \left(1 - \frac{|r_i - r_j|}{R_i + R_j} \right)^2.$$

To attain force balance we minimize the energy using the FIRE algorithm [3], under a constant imposed pressure. We then construct networks attaching the centers of overlapping particles with springs. The packings can then be discarded. For simplicity we set the spring constants to be unity and the initial rest lengths to be the interparticle distance, so that the initial networks are unstressed.

Details of networks

With the exception of the sequential materials we use two dimensional packing with approximately 500 nodes. Two dimensional systems allow us to study signaling (allostery) over long distances with relatively fewer nodes than three dimensions. The boundary conditions, for simplicity, are chosen to be periodic. For the nonmonotonic allosteric responses and the XOR gate the excess coordination number $\Delta Z = \frac{2N_B}{N} - 2d \approx 0.05$. Here, N_b is the number of bonds, N is the number of nodes and d is the dimensionality of the system. These spatially varying responses require a small ΔZ , where elasticity is anomalously long ranged[7, 17]. For the nonmonotonic global responses we use $\Delta Z \approx 0.15$ which is not particularly small. The networks for the sequential response are three dimensional with $\Delta Z \approx 0.4$. Unless indicated otherwise, we average over approximately 50 realizations.

TRAINING PROTOCOL

Following Ref. [12] we discretize the strain path to small steps. Every step consists of updating the strain, minimizing the elastic energy to attain force balance and then updating the rest lengths of springs. As discussed in the main text, the change in rest length is proportional to the stress on the bond:

$$\Delta \ell_{i,0} = \gamma k (\ell_i - \ell_{i,0}) \Delta t.$$

When the step size is made small then the dynamics may be considered quasistatic. We verify, that finer discretization does not alter our results.

APPENDIX B: DENSITY OF STATES

Convergence of training in the nonmonotonic responses exhibits a growing time scale as α is increased. One possible explanation for this is that low energy modes are created during training that compete with the trained path. To explore this possibility we consider the normal modes around the origin. The density of states $D(\omega)$ is defined as the number of modes in the range $[\omega, \omega + d\omega]$ divided by $d\omega$ and the number of particles. We focus on the integrated density of states $I(\omega) = N \int_0^\omega D(\omega') d\omega'$ shown in Fig. 4 since it allows us to count the number of low energy modes. For the untrained two dimensional system there are precisely two transnational zero modes due to the periodic conditions, and therefore $I(\omega)$ has a plateau at small frequencies. The trained systems have an additional near zero mode corresponding to the trained response, and therefore in that regime $I(\omega) \approx 3$. The trained configurations have an increased number of low energy modes in comparison to the untrained systems. Furthermore, increasing α also increases the number of low energy modes. This trend is most evident for $\alpha = 0, 1, 2$ though $\alpha = 3, 4$ are very close to $\alpha = 2$. While this is suggestive of this competing low energy mode picture, the density of states only characterizes infinitesimal deformations.

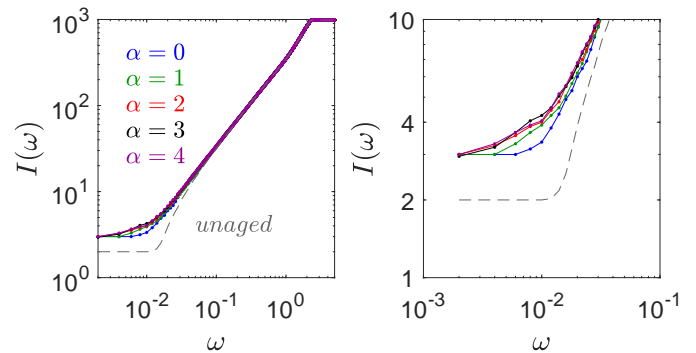


Figure 4. The integrated density of states. Left: over the entire frequency range. Right: zoom in at small frequencies. Larger α have an increased number of low energy modes in comparison to the small α curves.

-
- [1] Yohai Bar-Sinai, Gabriele Librandi, Katia Bertoldi, and Michael Moshe. Geometric charges and nonlinear elasticity of two-dimensional elastic metamaterials. *Proceedings of the National Academy of Sciences*, 117(19):10195–10202, 2020.
- [2] Katia Bertoldi, Pedro M Reis, Stephen Willshaw, and Tom Mullin. Negative poisson’s ratio behavior induced by an elastic instability. *Advanced materials*, 22(3):361–366, 2010.
- [3] Erik Bitzek, Pekka Koskinen, Franz Gähler, Michael Moseler, and Peter Gumbsch. Structural relaxation made simple. *Phys. Rev. Lett.*, 97:170201, 2006.
- [4] Bryan Gin-ge Chen, Nitin Upadhyaya, and Vincenzo Vitelli. Nonlinear conduction via solitons in a topological mechanical insulator. *Proceedings of the National Academy of Sciences*, 111(36):13004–13009, 2014.
- [5] Corentin Coulais, Eial Teomy, Koen de Reus, Yair Shokef, and Martin van Hecke. Combinatorial design of textured mechanical metamaterials. *Nature*, 535(7613):529, 2016.
- [6] Peter Dieleman, Niek Vasmel, Scott Waitukaitis, and Martin van Hecke. Jigsaw puzzle design of pluripotent origami. *Nature Physics*, 16(1):63–68, 2020.
- [7] Wouter G Ellenbroek, Ellák Somfai, Martin van Hecke, and Wim van Saarloos. Critical scaling in linear response of frictionless granular packings near jamming. *Physical review letters*, 97(25):258001, 2006.
- [8] Carl P. Goodrich, Wouter G. Ellenbroek, and Andrea J. Liu. Stability of jammed packings i: the rigidity length scale. *Soft Matter*, 9:10993–10999, 2013.
- [9] Carl P Goodrich, Andrea J Liu, and Sidney R Nagel. The principle of independent bond-level response: Tuning by pruning to exploit disorder for global behavior. *Physical review letters*, 114(22):225501, 2015.
- [10] Joseph N Grima and Kenneth E Evans. Auxetic behavior from rotating squares. *Journal of Materials Science Letters*, 19:1563, 2000.
- [11] Daniel Hexner, Andrea J Liu, and Sidney R Nagel. Role of local response in manipulating the elastic properties of disordered solids by bond removal. *Soft matter*, 14(2):312–318, 2018.
- [12] Daniel Hexner, Andrea J. Liu, and Sidney R. Nagel. Periodic training of creeping solids. *Proceedings of the National Academy of Sciences*, 2020.
- [13] Daniel Hexner, Nidhi Pashine, Andrea J Liu, and Sidney R Nagel. Effect of directed aging on nonlinear elasticity and memory formation in a material. *Physical Review Research*, 2(4):043231, 2020.
- [14] Yijie Jiang, Lucia M Korpas, and Jordan R Raney. Bifurcation-based embodied logic and autonomous actuation. *Nature communications*, 10(1):1–10, 2019.
- [15] Jason Z Kim, Zhixin Lu, Steven H Strogatz, and Danielle S Bassett. Conformational control of mechanical networks. *Nature Physics*, 15(7):714–720, 2019.
- [16] Roderic Lakes. Foam structures with a negative poisson’s ratio. *Science*, 235(4792):1038–1040, 1987.
- [17] Edan Lerner, Eric DeGiuli, Gustavo Düring, and Matthieu Wyart. Breakdown of continuum elasticity in amorphous solids. *Soft Matter*, 10(28):5085–5092, 2014.
- [18] Luuk A Lubbers and Martin van Hecke. Excess floppy modes and multibranch mechanisms in metamaterials with symmetries. *Physical Review E*, 100(2):021001, 2019.
- [19] James Clerk Maxwell. Iv. on the dynamical theory of gases. *Philosophical transactions of the Royal Society of London*, (157):49–88, 1867.
- [20] Anne S Meeussen, Erdal C Oğuz, Yair Shokef, and Martin van Hecke. Topological defects produce exotic mechanics in complex metamaterials. *Nature Physics*, pages 1–5, 2020.
- [21] Michael R Mitchell, Tsvi Tlusty, and Stanislas Leibler. Strain analysis of protein structures and low dimensionality of mechanical allosteric couplings. *Proceedings of the National Academy of Sciences*, 113(40):E5847–E5855, 2016.
- [22] Koryo Miura. Method of packaging and deployment of large membranes in space. *Title The Institute of Space and Astronautical Science Report*, 618:1, 1985.
- [23] Corey S. O’Hern, Leonardo E. Silbert, Andrea J. Liu, and Sidney R. Nagel. Jamming at zero temperature and

- zero applied stress: The epitome of disorder. *Phys. Rev. E*, 68:011306, 2003.
- [24] Nidhi Pashine, Daniel Hexner, Andrea J Liu, and Sidney R Nagel. Directed aging, memory, and nature's greed. *Science advances*, 5(12):eaax4215, 2019.
- [25] Matthew B Pinson, Menachem Stern, Alexandra Caruthers Ferrero, Thomas A Witten, Elizabeth Chen, and Arvind Murugan. Self-folding origami at any energy scale. *Nature communications*, 8(1):1–8, 2017.
- [26] Daniel R Reid, Nidhi Pashine, Justin M Wozniak, Heinrich M Jaeger, Andrea J Liu, Sidney R Nagel, and Juan J de Pablo. Auxetic metamaterials from disordered networks. *Proceedings of the National Academy of Sciences*, 115(7):E1384–E1390, 2018.
- [27] Jason W Rocks, Nidhi Pashine, Irmgard Bischofberger, Carl P Goodrich, Andrea J Liu, and Sidney R Nagel. Designing allostery-inspired response in mechanical networks. *Proceedings of the National Academy of Sciences*, 114(10):2520–2525, 2017.
- [28] Jason W Rocks, Henrik Ronellenfitsch, Andrea J Liu, Sidney R Nagel, and Eleni Katifori. Limits of multifunctionality in tunable networks. *Proceedings of the National Academy of Sciences*, 116(7):2506–2511, 2019.
- [29] Menachem Stern, Matthew B Pinson, and Arvind Murugan. The complexity of folding self-folding origami. *Physical Review X*, 7(4):041070, 2017.
- [30] Tomohiro Tachi and Thomas C Hull. Self-foldability of rigid origami. *Journal of Mechanisms and Robotics*, 9(2), 2017.
- [31] Le Yan, Riccardo Ravaio, Carolina Brito, and Matthieu Wyart. Architecture and coevolution of allosteric materials. *Proceedings of the National Academy of Sciences*, 114(10):2526–2531, 2017.
- [32] Mohamed Zanaty, Hubert Schneegans, Ilan Vardi, and Simon Henein. Reconfigurable Logic Gates Based on Programmable Multistable Mechanisms. *Journal of Mechanisms and Robotics*, 12(2), 02 2020. 021111.